A STUDY OF PULSATIONS IN A PLASMATRON WITH A SELF-STABILIZING ARC

A. S. An'shakov, G. Yu. Dautov, G. M. Mustafin, and A. P. Petrov

Zhurnal Prikladnoi Mekhaniki i Tekhnicheskoi Fiziki, Vol. 8, No. 1, pp. 161-166, 1967

ABSTRACT: Shunting is one of the basic processes which determine the properties of the arc and heated gas stream in a vortex plasmatron. Much attention has, therefore, been given recently to the character of the shunting mechanism and of the associated pulsations. The relationship between fluctuations of the flux brightness at the plasmatron outlet and the arc voltage is described in [1]. Paper [2] contains data on the effect of gas consumption and current on shunting frequency; it also shows the possibility of coexistence of several anode spots in an argon arc. The authors of [3] investigated the effect of electrode channel and electrode material polarities on arc voltage pulsations. In the present study we obtain voltage, current, and brightness distribution functions and reproduce oscillograms of these quantities and also of the current through the anode cross sections. We use various methods to prove the coexistence of several anode spots and discuss the effect of the intrinsic magnetic field of the arc on its behavior.

NOTATION

I, U are the time-average values of the arc current and voltage; I_n is the time-average current through the n-th anode cross section; I_{nt} is the instantaneous value of the variable component of the current through the n-th anode cross section; I_z is the time-average current per unit length of the anode; I_t, U_t, B_t are the instantaneous values of the variable components of the current, voltage, and jet brightness; I_s, U_s, B_s are the instantaneous values of the current, voltage, and jet brightness; f_u, f_i, f_b are the voltage, current, and jet brightness distribution functions; G is the gas consumption (flow rate) through the arc chamber; d is the inside diameter of the anode; t is the time; z is the coordinate along the arc chamber axis (whose origin lies at the cathode end face); ν_z is the time-average frequency of visitation of a unit anode length by an arc spot; ν_n is the time-average frequency of visitation of the n-th anode cross section by an arc spot; i, ν are the distribution functions of the quantities I_z and ν_z over the length of the anode; z_{0i}, $z_{0\nu}$ are the values of z corresponding to the maxima of i and ν; j is the current density in the arc column; **H is the intensity of the magnetic self-field of the arc;** s is the cross-sectional area of the arc column.

1. The experimental apparatus. The experiments were carried out on a standard single-chamber plasmatron (see diagram in Fig. 1). The anode consisted of mutually insulated segments of thickness 7 mm (the number of segments in our experiments was 16). The thickness of the zeroth segment was chosen in such a way that there was no shunting at the length z = b. The minimum gap between the cathode and zeroth segment was 1.5-2mm. The cathode was water-cooled, the anode air-cooled. A solid water-cooled anode was used in the experiments on the arc current and voltage and jet brightness distribution functions.

The quantities I and U were measured with LM-1 and E59 (class 0.5) instruments with scale ranges of 300 A and 600 V. The air consumption (flow rate) through the arc chamber was recorded by means of an RS-7 rotameter. In determining I_z as a function of z the time-average currents through the segments were measured with M-362 (class 1.5) ammeters.

Preliminary experiments showed the arc voltage in the segmented channel to be lower than in the continuous channel. It also turned out that this voltage difference diminished with increasing cleanness and smoothness of the surface of the segmented channel. The basic experiments using the plasmatron with the segmented anode were carried out at I = 70 A, G = 6 g·sec^{-1}, d = 1 cm. Under these conditions the arc voltage was 475 V in the case of the solid channel and 440 V in the case of the segmented channel, i.e., ΔU did not exceed 10% of the arc voltage in the continuous channel. Moreover, the oscillograms of U_t were of the same character in both cases. All of this indicates that the conditions of arc burning in a smooth segmented anode and a continuous anode are close, and that results obtained with a plasmatron with a segmented anode can be considered applicable to the case of a continuous anode. This is also the conclusion drawn by the authors of [2].

2. Distribution of I_z and ν_z over the length of the anode. The resulting distributions are shown in Fig. 2, where $i = I_z/I_{z\max}$, $\nu = \nu_z/\nu_{z\max}$.

In our computations we assumed that

$$\frac{I_z}{I_{z\max}} = \frac{I_n}{I_{n\max}}, \qquad \frac{\nu_z}{\nu_{z\max}} = \frac{\nu_n}{\nu_{n\max}}.$$

The frequency of visitation ν_n of a segment by an anode spot was determined with a VA-M-14 radiometer (sensitivity 0.3 V) by measuring the number of visitations over a 5-sec period. For this purpose a known resistance R_n was introduced into the circuit of each segment; the potential difference across the resistor was connected across the radiometer input terminals. The meter reading depended on R_n (the reason for this will be given below). The distribution of ν with respect to z shown in Fig. 2 was obtained for $R_n = 0.05$ ohm, $I_{n\max} = 18$ A, $\nu_{n\max} = 1.2 \cdot 10^4$ pulses/sec. Figure 2 shows experimental data for I = 70 A, U = 440 V, d = 1 cm, G = 6 g·sec^{-1}. We see from these curves that the functions i(z) and $\nu(z)$ are distributions of random quantities and are described by normal distribution laws

$$i(z) = e^{-k_i(z-z_{0i})^2}, \qquad \nu(z) = e^{-k_\nu(z-z_{0\nu})^2}. \tag{2.1}$$

In our case $k_i = 0.39$ cm^{-2}, $k_\nu = 0.33$ cm^{-2}, $z_{0i} = 15.05$ cm, $z_0 = 15.72$ cm. The solid curves were computed from formulas (2.1). For other values of I the shapes of these distributions remained the same, shifting toward smaller z with increasing current (as in the case of the cathode spot [4]). The quantities k_i, k_ν, z_{0i}, $z_{0\nu}$ in formulas (2.1) are functions of I, G, d, p. The maxima of i(z) and $\nu(z)$ do not coincide: $\nu(z)$ is shifted toward larger z relative to i(z). The reason for this can be seen from the oscillograms of Fig. 3, which were recorded by means of four OK-17M dual-beam oscilloscopes triggered synchronously to within $1 \cdot 10^{-6}$ sec. The time blips are common to all the oscillograms. From the oscillogram of U_t we see the gradual rise and then the rapid decline in U_t at the instant of shunting of the arc onto segment 2. The oscillograms of I_t can be considered to represent the absolute current through the segments, since the current of the non-self-sustaining discharge between the arc column and segment is small. Here we see the successive transitions of the anode spot from one segment to the next in the direction of gas flow. The current pulses at the first segments are stable and of long duration.

The position of the spot becomes less stable as it moves in the direction of gas flow. For example, at the sixth segment the spot appears, vanishes, and reappears almost immediately (this is clear from the shape of I_{6t}). Moreover, the length of time for which the spot remains in each segment diminishes; this is partly attributable to the increase in gas velocity along the arc and to the looping of the arc end. The signals from the final segments become weak but fairly frequent. The VA-M-14 radiometer received both the powerful and long signals from the first segments and the short weak signals from the last segments as discrete pulses. This explains the shift in $\nu(z)$ relative to i(z). With increasing R_n the radiometer recorded weaker and weaker signals. This meant that the shift in $\nu(z)$ relative to i(z) also depended on R_n.

The oscillograms of Fig. 3 enabled us to find the velocity of the anode spot in the axial direction. This velocity is defined as the ratio of the segment thickness to the time of presence of the spot in the

segment. At the beginning of the shunting zone it was 170 $msec^{-1}$. The mass-average gas velocity at the plasmatron outlet was approximately 750 $msec^{-1}$.

Small-scale shunting of the arc-electrode type along the line DC (Fig. 1) ensured discontinuous displacement of the anode spot along the electrode surface. Here channel DB dies out while channel DC develops. This is evident, for example, from the gradual decline in I_{2t} and growth in I_{3t} as the spot passes from the second segment to the third. Two spots naturally exist at such instants. However, two spots often coexist at far-removed segments as well. We obtained oscillograms which revealed the simultaneous progression of two anode spots over a distance equal to the thickness of three sections. The coexistence of several anode spots was further confirmed by means of an SSA apparatus for recording coincidences and anticoincidences with a resolving time of 10^{-6} sec. The instrument counted the cases in which anode spots were present at two segments simultaneously.

The experiment was carried out for b = 8.5 cm, I = 60 A, U = = 450 V, ΔU = 45 V, G = 6 g·sec^{-1}, d = 1 cm.

The numbers N of the segments from which the signals were recorded and the numbers n of signal coincidences over a period of t = 5 sec were as follows:

N	11,12	11,13	11,14	12,14	11, 12, 13	11, 12, 14	11, 12, 13, 14
n	1570	2850	3900	2560	90	230	70

Finally, our photographs of the arc chamber taken from the end of the continuous anode (Fig. 4) using an SFR operating as a time lens (speed: $6 \cdot 10^4$ frames/sec) also confirm the coexistence of several anode spots. The frames of Fig. 4 were used to determine the velocity of rotation of the radial portion of the arc, which turned out to be on the order of 1800 rps.

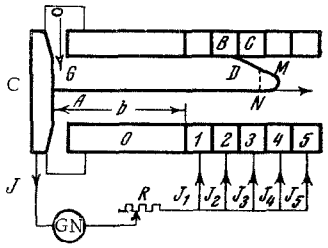

Fig. 1. Diagram of the plasmatron. 0–5 = anode segments, C = cathode, Gn = generator, R = resistor, AB = arc, G = gas intake.

3. The voltage, current, and jet brightness distribution functions. Figure 5 shows oscillograms of the variable components of the arc current, arc voltage, and jet brightness at a distance of 1–1.5 mm from the end of the anode. By the brightness we mean the integral jet radiation flux incident on the photomultiplier. We measured B_t with an FEU-19 photomultiplier. The oscillograms were recorded with a DESO-1 dual-beam cathode-ray oscilloscope with inactive horizontal scan. The position of the beams was photographed off the screen with an FR-11 camera, which yielded long-duration oscillograms. From these oscillograms we see that the shunting frequencies and the quantities I_t, U_t, B_t were not periodic, exhibiting random deviations from their average values. This led us to take the usual step of introducing distribution functions to characterize the process. For example, the probability of the voltage $U_s = U + U_t$ lying in the interval from U_s to $U_s + dU_s$ can be expressed in terms of f_u:

$$d\Gamma_u = f_u\, d\, U_s. \tag{3.1}$$

The normalized function f_u can be approximated from the oscillograms. To this end we divide the duration of the oscillogram into m equal segments and determine the number m_s of segments where U_s lies in the range from U_s to $U_s + \Delta U_s$. Then $\Delta\Gamma_u = m_s/m$, and we find from (3.1) that

$$f_u = m_s / m\Delta\, U_s. \tag{3.2}$$

Next, we determined f_u, f_i, f_b. The resulting functions conform to the normal distribution laws

$$f_u = \sqrt{l_u/\pi}e^{-l_u(U_s-U_0)^2},\quad f_i = \sqrt{l_i/\pi}e^{-l_i(I_s-I_0)^2}$$
$$f_b = \sqrt{l_b/\pi}e^{-l_b(B_s-B_0)^2}. \tag{3.3}$$

Here I_0, U_0, B_0 are the arithmetic means of I_S, U_S, B_S. In the case of normal distributions the arithmetic means of the current and

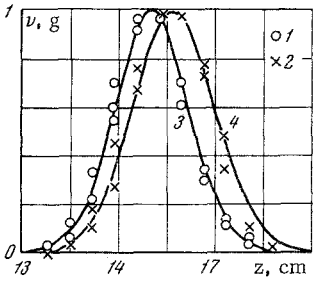

Fig. 2. Distributions of the relative current density i and relative frequency ν of segment visitation by an anode spot with respect to anode length. 1 and 2 are the experimental points for i and ν; 3 and 4 are the normal distributions according to formulas (2.1); I = 70 A, U = 440 V, G = 6 g·sec^{-1}, d = 1 cm.

voltage are equal to the readings of the moving-coil instruments, i.e., $I_0 = I$, $U_0 = U$. For I = 110 A, U = 412 V, G = 6 g·sec^{-2}, d = 1 cm. The coefficient l_u is equal to $10^{-2} \cdot 3.3\ V^{-2}$.

Figure 6 shows the resulting distribution functions, where x represents (U_S – U), (I_S – I), (B_S – B). One division along the x axis

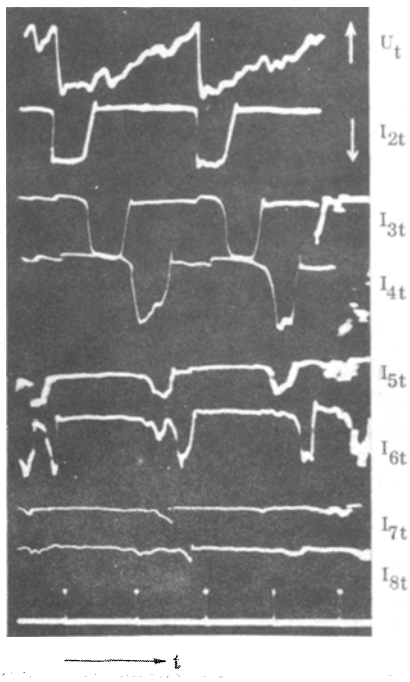

Fig. 3. Oscillograms of the variable components of the voltage arc current I_t through the anode U_t and sections. Time blips represent 10^{-4} sec intervals, I = 83 A, U = 375 V, G = g·sec^{-1}, d = 1 cm, b = 8.5 cm; segment thickness 0.7 cm.

represents 6 V, and the values of (I_S – I) and (B_S – B) are given in arbitrary scales. For convenient plotting we multiplied them by the

quantities

$$\sqrt{\pi/l_u},\ \sqrt{\pi/l_i},\ \sqrt{\pi/l_b},$$

respectively.

The solid curves were constructed from formulas (3.3), while the experimental points were obtained from the oscillograms and converted using formula (3.2). As we see, the experimental data are described well by normal distributions (3.3). Thus, both the functions i(z), ν(z), and f_u, f_i, f_b under our conditions conformed to a random distribution, and the shunting mechanism depended on random perturbations. These perturbations take the form of fluctuations of the temperature, velocity, pressure, and other quantities as a result of turbulent pulsations, fluctuations of the electrical parameters, etc.

Knowing the distribution functions, we were able to determine the values of the required quantities without difficulty. Thus, the mean square value of the fluctuation amplitude ΔU_1^2 is given by the formula

$$\Delta U_1^2 = \int_{-\infty}^{\infty} x^2 f_u(x)\,dx, \qquad f_u(x) = e^{-l_u x^2}\left(\frac{l_u}{\pi}\right)^{1/2}.$$

Let us consider some of the characteristic features of current pulsations. The current variation in Fig. 5 resembles the mirror image of the voltage variation. The difference lies in the fact that substantial perturbations of a frequency on the order of $5 \cdot 10^4$ cps are superimposed on the current pulsations, which are associated with large-scale longitudinal shunting. Moreover, the shape of the oscillogram of I_t depends markedly on the power source and on the electrical circuit parameters.

4. The effect of the positive column loop on arc behavior. Under the action of the stream of heated gas the radial portion of the arc experiences deformation into the loop BN (Fig. 1), rotates about the electrode axis, and at the same time moves in the direction of axial flow of the gas. Formation of the loop and its shunting along the line NM are easily observable if the electrode is made so short that the loop extends beyond the electrode. Figure 7a shows photographs of a loop recorded with an SKS-1 motion picture camera at a speed of $4 \cdot 10^3$ frames/sec. The anode in these photographs is on the left-hand side; the arc emerges from the anode, forms a loop, and returns to the anode (to the lower portion of its end face). Shunting of the loop by the newly-formed shorter current-conducting channel can be seen in the second and sixth frames.

This looping effect results in complex interaction of the arc with its magnetic self-field. To investigate this let us consider the simplest case where the diameter of the arc column is constant and where its axis is a line in the plane of the diagram (Fig. 7b). The force acting on a unit length of the column is

$$\mathbf{F} = \int_s [\mathbf{jH}]\,ds$$

which lies in the plane of the figure and is directed perpendicularly to **j**. Figure 7b is a qualitative picture of the distribution of **F** for the arc ACB. The force **F** obliges the arc to move relative to the gas stream, so that we can expect the following picture of motion of the arc ACB. Over the segment BC the projection of **F** on the r-axis is partly compensated by the stabilizing effect of the rotational motion of the gas. The motion of the loop in the z-direction is limited only by the aerodynamic drag of the gas; the velocity of its relative motion, which depends on the current and on other conditions, can be considerable. Under the action of **F** the segment SL sags below the z-axis. The distortion in the neighborhood of S in turn forces the arc segment PS upwards, etc. Since the arc simultaneously rotates about the z-axis, the force **F** results in oscillations of the arc end in the shunting zone. This appears to be a partial explanation of the transverse oscillations of the arc end reported in [5].

The formation of a prolate loop favors the growth of the frequency of arc-electrode shunting along the line DC (Fig. 1) at the end of the shunting zone.

This is confirmed by the reduced time of presence of the anode spot in segments lying near the end of the shunting zone (e.g., compare the durations of the pulses I_{2t} and I_{6t} in Fig. 3).

The marked effect of the magnetic self-field of the arc on its behavior is especially obvious for large currents. Figure 7c is a series of photographs of the motion of the two radial portions of an arc in the inside electrode of a two-chamber vortex plasmatron in an argon medium (d = 7 cm, G = 160 g·sec^{-1}, I = 1800 A). These photographs show clearly how the interaction of the magnetic fields of the two radial portions reduces the velocity of the front current-conducting channel and increases that of the rear channel. The channels then merge. This shows that the forces in the magnetic self-field sometimes become comparable with the force exerted by the stream on the arc.

Allowance for the effect of the magnetic self-field in the loop zone enables us to explain yet another phenomenon. The arithmetic mean distance z_{0i} between the cathode and anode loops for the mode of plasmatron operation shown in Fig. 2 is equal to approximately 15 cm. If the arc does not have a loop and is well stabilized along the electrode axis, then the voltage of an arc of this length is 330 V [6]. The mean potential drop across the loop is then on the order of 110 V. This value is too large, even if we allow for the low temperature of the gas at the electrode walls. As we know [7], the motion of the arc relative to the arc axis results in a considerable rise of the electric field intensity.

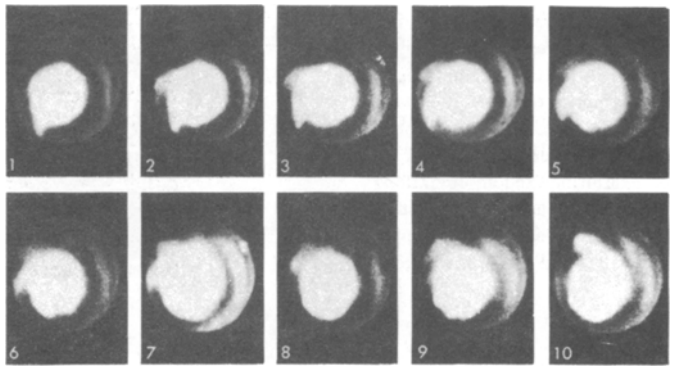

Fig. 4. Photographs of the arc chamber taken from the end of the solid anode. The numbers indicate the sequence of frames. I = 105 A, G = 6 g·sec^{-1}, d = 1 cm.

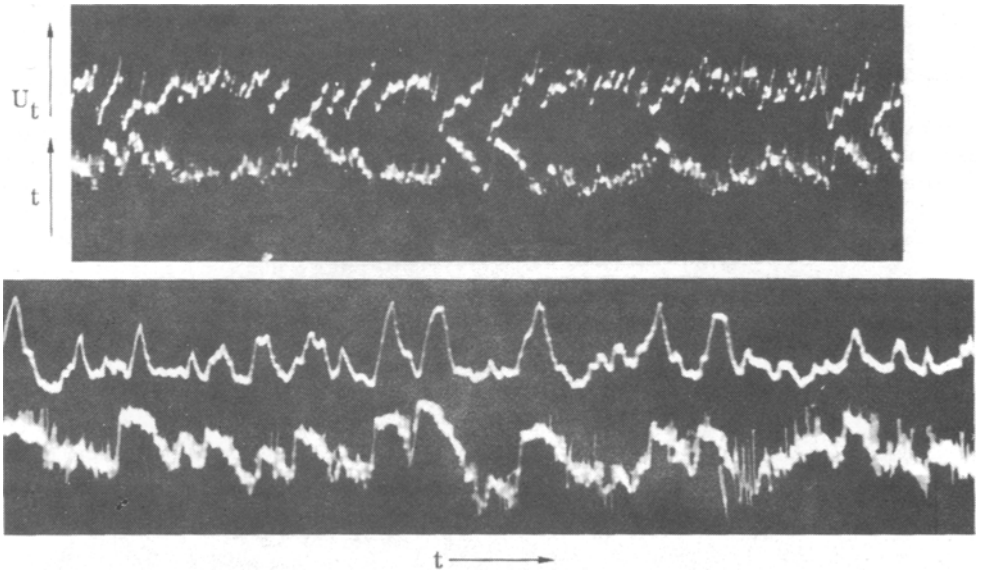

Fig. 5. Oscillograms of the variable components of the voltage, current, and jet brightness for I = 110 A, U = 412 V, G = 6 g · sec^{-1}, d = 1 cm. The duration of the scans is $5.6 \cdot 10^{-3}$ sec.

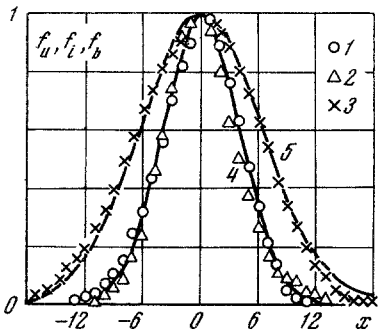

Fig. 6. Voltage, current, and jet brightness distribution functions at the plasmatron outlet. 1, 2, and 3 are experimental points for the voltage, current, and brightness, respectively; 4 is the theoretical voltage and current curve; I = 110 A, U = 412 V, G = 6 g · sec^{-1}, d = 1 cm.

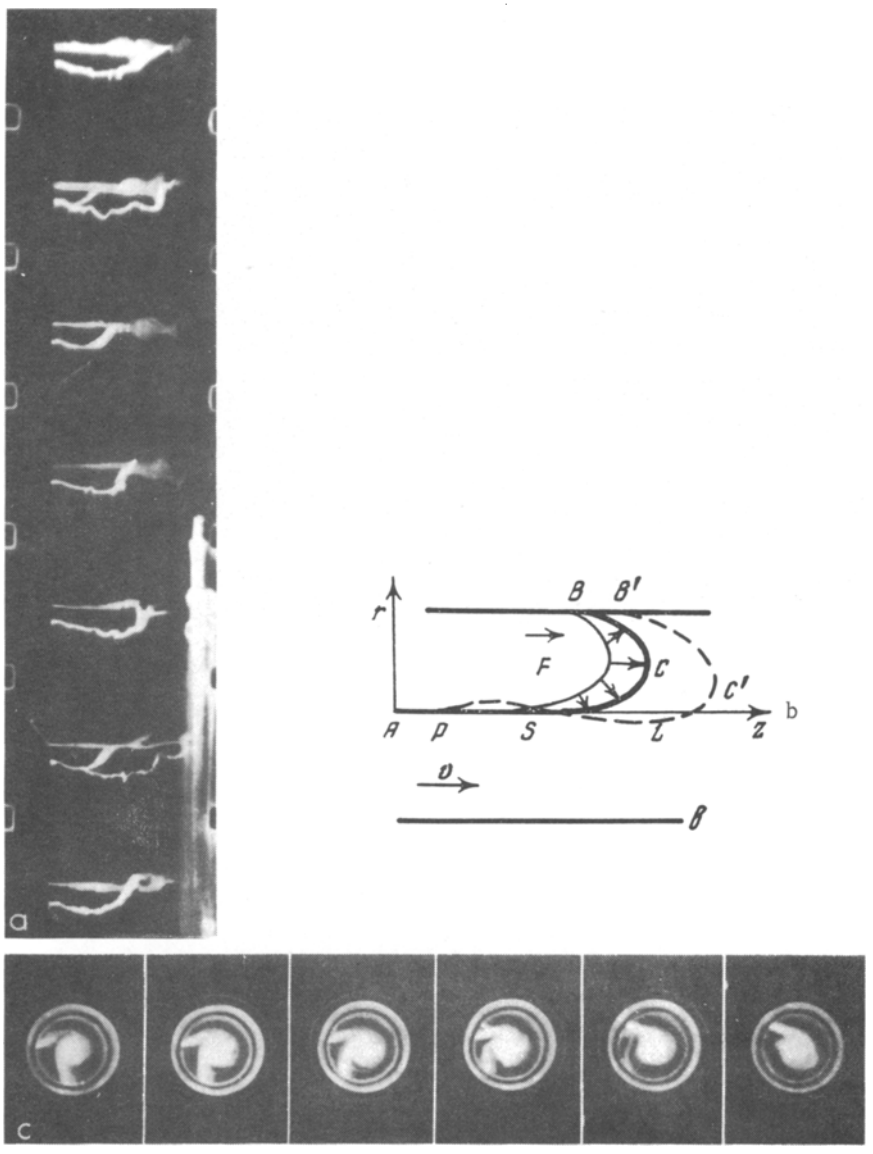

Fig. 7. a) Photograms of the arc loop emerging from the anode. Camera speed: $4 \cdot 10^3$ frames/sec, d = 3.5 cm, I = 50 A, G = 27 g · sec^{-1}; air medium; direct polarity; b) distribution of the electrodynamic force **F** for the arc loop; c) photographs of the motion of the two radial portions of the arc in the inside electrode of a two-chamber vortex plasmatron. G = 160 g · sec^{-1}, I = 1800 A, d = 7 cm. Camera speed: $4 \cdot 10^3$ frames/sec.

We can, therefore, assume that in this case the deformation and relative motion of the arc under the action of the magnetic self-field are among the reasons for the large potential drop in the arc loop zone.

The authors are grateful to Yu. S. Dudnikov for his assistance.

REFERENCES

1. G. R. Jorden and L. A. King, "The nature of fluctuations present in dc plasma jets in argon and nitrogen," Brit. J. Appl. Phys., vol. 16, no. 4, 1965.

2. J. Moritz, W. Neumann, and K. Rademacher, "Über die Bewegung des Bogenansatzes an Plasmastrahl-Hohlanoden," Beitr. Plasma Phys., vol. 5, no. 4, 1965.

3. V. O. German and M. G. Morozov, "A dc plasmatron and some results obtained in investigating its operation," Teplofizika vysokikh temperatur, vol. 2, no. 5, 1965.

4. G. Yu. Dautov and M. F. Zhukov, "Some generalizations of studies of electric arcs," PMTF [Journal of Applied Mechanics and Technical Physics], no. 2, 1965.

5. A. M. Trokhan, "A photographic study of pulsations in air-stabilized plasmatrons," PMTF, no. 2, 1964.

6. G. Yu. Dautov, Yu. S. Dudnikov, M. F. Zhukov, and M. I. Sazonov, "Distribution of the potential along the arc in a vortex plasmatron," PMTF [Journal of Applied Mechanics and Technical Physics] no. 5, 1965.

7. O. B. Bron, Electric Arcs in Control Apparatus [in Russian], Gosenergoizdat, 1954.

9 March 1966 Novosibirsk